ACCEPT/REJECT CRITERIA FOR STRUCTURAL CERAMICS:

PART 1: SOME EFFECTS OF CAVITIES ON THE FRACTURE OF CERAMICS
I. CYLINDRICAL HOLES

A. G. Evans
Rockwell International Science Center
Thousand Oaks, California 91360

D. R. Biswas and R. M. Fulrath
Materials and Molecular Research Division
Lawrence Berkeley Laboratory and Department of Materials Science
and Mineral Engineering, University of California,
Berkeley, California 94720

ABSTRACT

The problem of fracture from cylindrical cavities in brittle materials has been analyzed. The analysis is based on the conditions required to extend cracks that pre-exist at the cavity surface. It involves the combined use of fracture mechanics and statistics solutions for crack extension in the concentrated stress field around the cavity. The general pertinence of the approach is substantiated by experimental studies of fracture from cavities in polycrystalline alumina.

INTRODUCTION

The fracture of ceramic components frequently initiates at holes or voids,[1] and it is of considerable practical importance to comprehend the detailed influence of cavities on fracture initiation.

Fracture from cavities is most realistically treated by examining the extension of flaws at (or near) the cavity surface.[1,2] The flaws are considered to extend when the stress intensity, due to the combined stress field of the cavity and the flaw, attains the critical value for local crack extension. The flaw responsible for fracture in polycrystalline ceramics may either pre-exist or may develop due to subcritical extension of grain boundary cusps. In either case, a distribution of flaws should exist, prior to final fracture, in the vicinity of the cavity surface. The analysis of fracture from cavities is thus a statistical problem, involving the extension of crack arrays in localized stress fields. A preliminary attempt to address this problem[3] has used the unperturbed stress field at the cavity surface as the basis for the statistical analysis. This analysis only pertains, of course, when the cracks are small enough (vis-a-vis the cavity radius) that stress gradient effects across the crack and interaction effects[2] can be neglected.

Further progress in the characterization of fracture from cavities requires that the statistical approach be extended to include the entire range of crack sizes of practical concern (up to at least half the cavity radius)[1,4] and hence to incorporate the stress gradient and interaction effects on crack propagation. Three-dimensional stress intensity factor solutions for cracks emanating from the cavity surface# are needed for this purpose. These results can then be combined with statistical crack size distributions to obtain the appropriate fracture relationships. The present paper considers the problem of fracture from cylindrical cavities; while a companion paper examines the analagous problem of fracture from spherical cavities. These papers emphasize the basic approach for combining linear elastic fracture mechanics solutions with statistical results. For this purpose, the best available fracture mechanics and statistical analyses are invoked; recognizing that, in some instances, the solutions are still rather approximate. Evidently, improved solutions can be incorporated, as they emerge, using the same basic procedures.

To ascertain the general validity of the analytic results, it is required that cavities with well-defined surface crack distributions be prepared and tested. Preliminary results are obtained in this study by performing experiments on a hot pressed polycrystalline alumina containing cylindrical cavities.

STRESS INTENSITY FACTOR SOLUTIONS

Well-established stress intensity factor K solutions can be obtained directly from the literature for the two-dimensional problem of single (or double) radial cracks emanating from a cylindrical hole[5] (Fig. 1). However, there are few well-substantiated solutions for the more relevant three-dimensional problems, such as semi-elliptical cracks at the surface of cylindrical cavities. Approximate three-dimensional solutions are often obtained by linear superposition. Such solutions are particularly convenient to derive, and are the primary solutions used in the present studies. Hence, the methods of solution and the expected accuracy of the results are examined.

#A similar approach can be used to include volume cracks that do not terminate at the cavity surface. However, the analysis is complicated by subcritical crack/cavity linking effects, and the analysis is thus deferred to a subsequent publication.

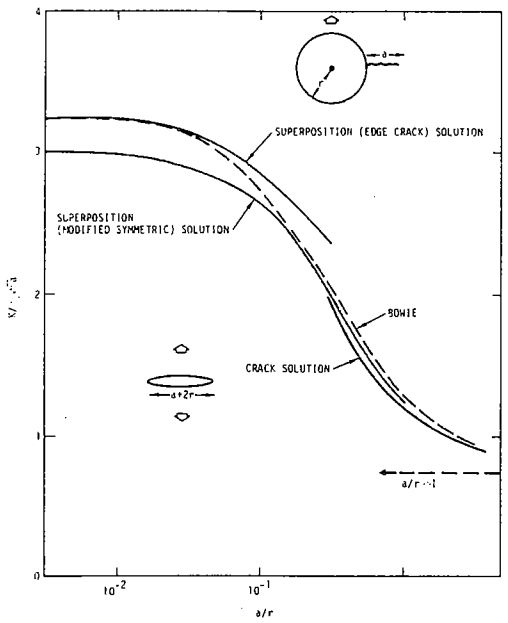

Fig. 1. Stress intensity factor solutions for a single radial crack emanating from a cylindrical hole.

The three primary superposition results are: for a two-dimensional symmetrically loaded crack of length 2a,[6,7]

$$K_I = \frac{1}{(\pi a)^{\frac{1}{2}}} \int_{-a}^{a} \sigma_\theta(z) \left(\frac{a+z}{a-z}\right)^{\frac{1}{2}} dz \qquad (1)$$

where z is the distance from the crack center and σ_θ is the tensile stress normal to the crack: for a two-dimensional edge crack of length a[8]

$$K_I = 2\left(\frac{a}{\pi}\right)^{\frac{1}{2}} \int_{0}^{a} \frac{[1 + F(z/a)]}{(a^2 - z^2)^{\frac{1}{2}}} \sigma_\theta(z) dz \qquad (2)$$

where, $F(z/a) = (1-z/a)[0.29-0.39(z/a)^2 + 0.77(z/a)^4 - 0.99(z/a)^6 + 0.59(z/a)^8]$: for a three-dimensional fully-contained crack[6,7,9]

$$K_I\Big|_{\psi=0} = \frac{2}{(\pi a)^{3/2}} \int_{0}^{\pi} \int_{0}^{a} \frac{y[1-(y/a)^2]^{\frac{1}{2}} \sigma(y,\psi)}{[1-2(y/a)\cos\psi + (y/a)^2]} dy\, d\psi \qquad (3)$$

where y is the radial distance from the crack center, and ψ is the angular coordinate with reference to the crack front location of interest (see Fig. 2).

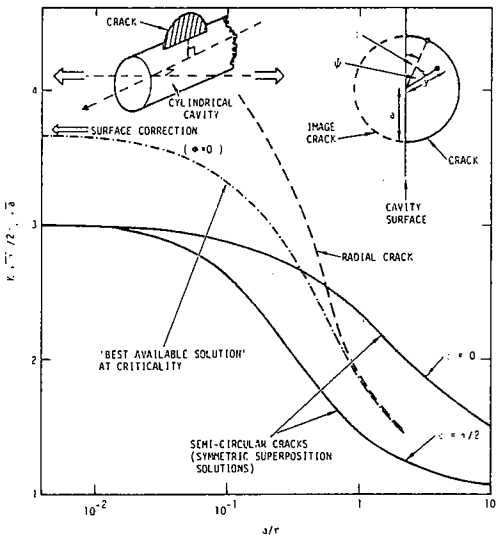

Fig. 2. Stress intensity factor solutions a semi-circular crack on the surface of a cylindrical cavity.

To examine the expected utility of the superposition method, a solution is derived for the radial crack configuration shown in Fig. 1. The tangential stress $\sigma_\theta(x)$ around a cylindrical cavity (radius r) normal to the applied stress σ_∞ is,[10]

$$\sigma_\theta = \sigma_\infty \left[1 + \frac{1}{2}\left(\frac{r}{r+x}\right)^2 + \frac{3}{2}\left(\frac{r}{r+x}\right)^4\right] \qquad (4)$$

where x is the distance from the cavity surface. Substituting Eqn. (4) into Eqns. (1) and (2) (and applying a single crack correction[7], $[(2r+a)/(2r+2a)]^{\frac{1}{2}}$ to convert the symmetric double crack solution to a single crack solution) yields the results plotted in Fig. 1. Also shown is the result for a crack of equivalent length (a+2r). It is apparent that the modified symmetric solution affords a very good approximation in the range $a/r \gtrsim 0.2$, as observed by Shah[7]; whereas the edge crack solution provides a superior correlation for smaller a/r. Carefully chosen superposition solutions thus appear to provide stress intensity factor approximations that should be satisfactory for present purposes.

The three-dimensional configuration of interest for the present statistical analysis is the semi-circular crack on the surface of a cylindrical cavity (Fig. 2). An approximate superposition solution for this problem considers a circular crack symmetrically loaded about the cavity surface, by the stress field of the cavity (Eqn. 4); i.e., it invokes an image crack within the cavity (Fig. 2). The solution is obtained by replacing x in Eqn. (4) with $y \sin[\phi+\psi]$ (ϕ is the angle defined in Fig. 2), substituting Eqn. (4) into Eqn. (3), and integrating. The results are plotted in Fig. 2 for crack front locations both coincident with the cavity surface

(ϕ=o) and remote from the cavity (ϕ=π/2). The stress intensity factors are in close agreement with those derived by Shah,[7] using a similar analysis. These solutions must be corrected for the presence of the cavity surface. The surface corrections for small a/r should be of the same order as those obtained for uniformly stressed surface cracks.[8] The correction for remote crack front locations (ϕ=π/2) is small, ~1.03; while for near surface locations# (ϕ ~o) the correction is relatively large, ~1.23, as indicated on Fig. 2. Allowing for possible surface corrections of this magnitude, a comparison of the surface crack solutions plotted in Fig. 2 with the radial crack solution (transposed from Fig. 1) indicates that, for relatively large cracks (a/r $\gtrsim$ 1), the stress intensity factor for a semi-circular crack (at ϕ=o) is substantially larger than that for a radial crack of equivalent length. Semi-circular surface cracks in this size range should thus extend subcritically, into radial cracks (or more likely, into an intermediate semi-elliptical configuration) before propagating to fracture. For small a/r, the stress intensity factors for semi-circular cracks are lower than for radial cracks, indicating that semi-circular cracks in this size range should propagate unstably to fracture. The "best available solution" for the stress intensity factor at criticality should thus exhibit the approximate form depicted in Fig. 2. A functional expression for this curve which is convenient for subsequent analysis (derived using a formulism proposed by Grandt)[11] is given by:

$$\frac{K_I \sqrt{\pi}}{2\sigma_\theta \sqrt{a}} = 1.07 + \frac{1.37}{0.52 + a/r} \qquad (5)$$

One other type of crack that is of interest for the cylindrical cavity problem is the corner crack (Fig. 3). Stress intensity factor solutions for this configuration[12] indicate that K will be augmented near the free surface intersection, by ~1.33. This correction will be applied when fracture is expected to initiate from corner cracks.

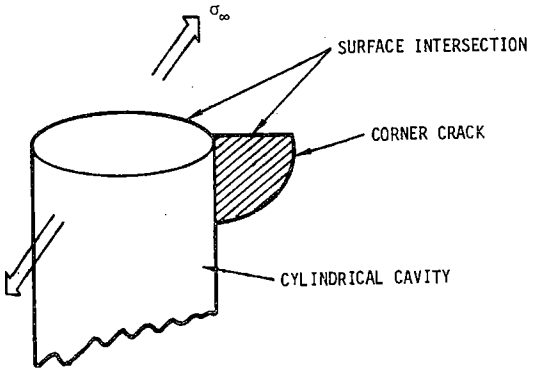

Fig. 3. A schematic of a corner crack.

#The singularity at the surface, ϕ=o, tends to zero[8]; but increases rapidly for $\phi > 0$, to a maximum at ~0.05π .

FRACTURE STATISTICS

The probability of fracture $\Phi(S)$ when fracture occurs by the unstable extension of non-interacting surface cracks is, in general, related to the state of stress, S, by[13];

$$\ell n[1-\Phi(S)] = \int_A dA \int_o^S g(S)dS \qquad (6)$$

where A is the stressed area and g(S)dS is the number of flaws in unit area that extend unstably in the stress range S to S + dS. The function g(S) can be deduced from experimental strength data[3,4] and usually, several flaw populations exist over the entire strength range[4] (0 $\rightarrow \infty$); so that several functional forms are needed to fully-describe g(S). However, for a restricted range of strength, the mathematically convenient reduced Weibull function[5] is usually found to afford an adequate description;

$$\int_o^S g(S)dS = \left(\frac{S}{S_o}\right)^m \qquad (7)$$

where m is a shape parameter and S_o a scale parameter. This fracture probability relation can be used in conjunction with stress fields at cavity surfaces and K solutions to obtain expressions for cavity fracture. Some caution should be exercised, however, when the subcritical extension of surface cracks is involved (see Section 2), because this phenomenon can lead to instability conditions that violate the postulates used to derive Eqn. (6).

For a cylindrical cavity with a stress applied normal to the cylinder axis (Fig. 4) the stress at the cavity surface is biaxial[10] (except for the small plane stress condition near the ends). The tangential stress σ_θ is given by[10];

$$\sigma_\theta = \sigma_\infty[4\sin^2\theta - 1] \qquad (8)$$

where θ is the location on the cavity surface with respect to the applied stress axis. The longitudinal stress σ_z (Fig. 4) is equal to $\nu\sigma_\theta$.[10] Both stresses are thus tensile in the range, $5\pi/6 > \theta > \pi/6$.

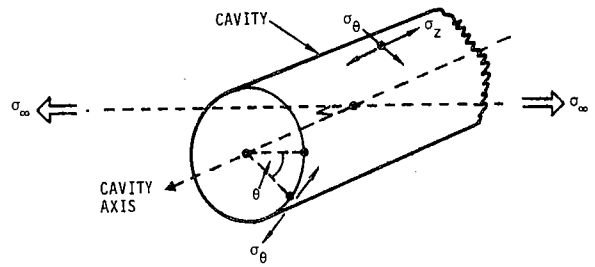

Fig. 4. A schematic indicating the configuration used for statistical analysis.

Fracture is considered to be restricted to the tensile region, because the crack extension stress under biaxial compression substantially exceeds that under biaxial tension.[6] In the tensile range, the pertinent strength distribution function is that which pertains to a principal stress ratio S_1/S_2 equal to ν. For the function given by Eqn. (7),[7] it has been demonstrated[7] that probabilities of fracture in multiaxial tension can be related to those in uniaxial tension through a proportionality term $I(m, \nu, S_1/S_2)$; the fracture probability being greater in multiaxial tension than in uniaxial tension. This proportionality is contained in subsequent calculations of the fracture probability. The modified strength distribution is thus

$$\int_0^{S_1} g(S_1)dS_1 = I(m,\nu,S_1/S_2)\left(\frac{S_1}{S_o}\right)^m \qquad (9)$$

where S_1 is the maximum principal tensile stress. Hence, for very small cracks at the cavity surface ($a/r < 10^{-2}$) the fracture probability derived from Eqns. (6) to (9) by equating S_1 to σ_θ is,

$$-\ell n[1-\Phi(S_\infty)] = 4rt\left(\frac{S_\infty}{S_o}\right)^m I(m,\nu)\int_{\pi/6}^{\pi/2}(4\sin^2\theta-1)^m\,d\theta$$

$$\equiv 4rt\,A(m)(S_\infty/S_o)^m \qquad (10)$$

where S_∞ is the magnitude of the applied stress σ_θ at fracture and t is the length of the cylindrical cavity. For $S_1/S_2 = \nu = 0.2$, inserting the proportionality $I(m,\nu)$ derived from Ref. 7 into Eqn. (10) and integrating yields the A(m) plotted in Fig. 5.

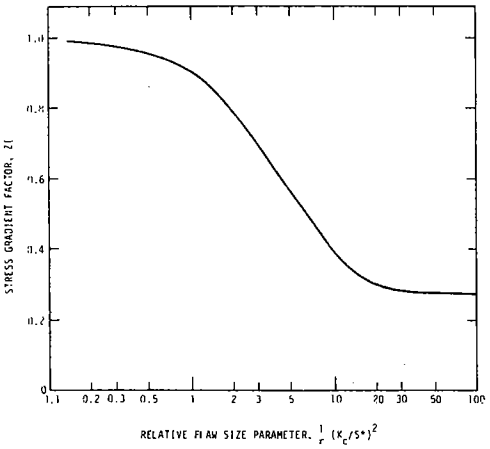

Fig. 5. The dimensionless fracture probability factor A(m) for fracture from a cylindrical cavity, plotted as a function of the shape parameter m of the flaw size distribution. Note that A(m) can be approximately expressed by $A(m) \sim 0.35\exp(1.06m)$.

For larger a/r, this result must be modified to account for stress gradient effects. The K solution that reflects the crack extension condition at instability (see Section 2) should be used for this purpose. For flaws normal to the applied stress, K_I in Eqn. (5) can be equated to the critical value K_c#, to obtain the effective flaw strength S* (i.e., the applied stress required to cause unstable crack extension), which can then be expressed in terms of the apparent strength S (that obtained by assuming uniform tension near the cavity surface, $S = \sqrt{\pi}\ K_c/7.38\sqrt{a}$) as (Appendix I);

$$\frac{S}{S^*} = 0.33 + 2B(0.11 - 0.056\alpha)^{\frac{1}{2}} \equiv Z(\alpha) \qquad (11)$$

where

$B = \cos(\beta/3)$, $\cosh(\beta/3)$ or $\sinh(\beta/3)$, $\cos\beta$, $\cosh\beta$,

$$\sinh\beta = (0.037 - 0.004\alpha)/(0.11 - 0.056\alpha)^{3/2}$$

and

$$a = \frac{1}{\pi}\left(\frac{K_c}{S^*}\right)^2$$

The choice of the cos, cosh or sinh relation for B depends on the magnitude of α, in the usual way. The stress gradient factor $Z(\alpha)$ given by Eqn. (11) is plotted in Fig. 6.

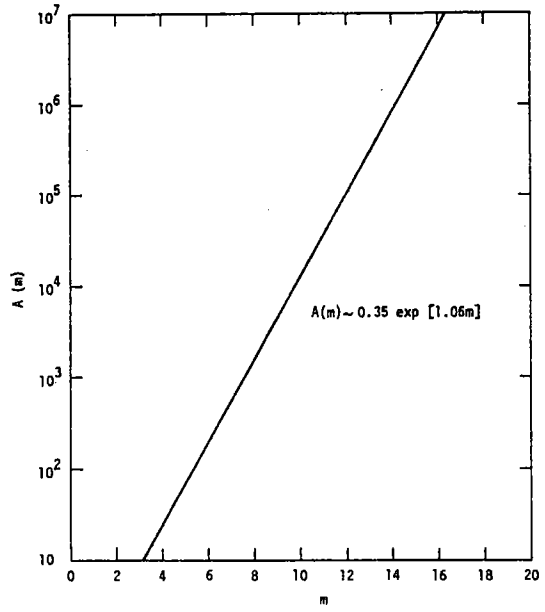

Fig. 6. The stress gradient correction term.

#Herein we assume that K_c is independent of crack length. This is not valid for cracks comparable in size to the microstructural dimensions.[1,2]

We now assume that a similar relation between S and S* pertains for all flaws in the tensile range (i.e., that the stress gradient is relatively insensitive to the flaw location and orientation). The fracture probability can then be obtained by substituting S from Eqn. (11) for S_∞ in Eqn. (10), to give;

$$-\ell n\left[1-\Phi(\hat{S}_\infty)\right] = 4rt\left(\frac{\hat{S}_\infty}{S_o}\right)^m Z^m(\alpha) \qquad (12)$$

where $\hat{S}_\infty$ is the new value of the applied stress at fracture. Before proceeding, it is important to examine the implications of the assumption concerning the orientation independence of the stress gradient factor. An exact solution to the present problem would require that K_I, K_{II}, and K_{III} solutions be derived (for $5\pi/6 > \theta > \pi/6$) for all possible flaw locations and orientations at instability; and then to derive the equivalent S/S* functions. This is too extensive an exercise to attempt for present purposes. But it is instructive to develop a qualitative appreciation of the probable trends. For all flaw orientations within a specified element, $d\theta$ (Fig. 4), the two stresses σ_θ and σ_z are interrelated ($\sigma_z = \nu\sigma_\theta$). The stress gradient factor for given θ should, therefore, be orientation independent. The only substantive differences might occur at large a/r, where cracks with normals parallel to the cylinder axis (Fig. 4) tend to an annular shape at criticality, rather than the radial configuration analyzed in Section 2. However, these cracks are in an unfavorable orientation for extension in the present problem, and do not provide an appreciable contribution to the fracture probability. The effect of the axial orientation, θ, on the stress gradient factor may be surmized by examining the tangential and shear stress distributions.[10] The tangential stress gradient (and hence, the K_I gradient) decreases with rotation away from $\theta = /2$, because the importance of the $(r+x)^{-4}$ term in Eqn. (4) diminishes. However, this tends to be counteracted by the emergence of a shear stress (or K_{II} component) with a strong $(r+x)^{-4}$ term. The orientation dependence of the stress gradient factor could, therefore, be relatively small.

The trends in the fracture probability with the relative strength $\hat{S}_\infty/S_o$, predicted by Eqn. (12) are plotted in Fig. 7 as a function of the relative cavity size (r/r_o), for a typical flaw size variability m of 4; the figure was constructed by letting $r_o t$ and $K_c^2/r_o S_o^2$ be unity. Also plotted on the figure are the fracture probabilities $\Phi(S_\infty)$ obtained from Eqn. (12) for the uniform tension case. It is apparent from Fig. 7 that the fracture probability deviates from the uniform stress result at low strengths (large a/r) and that the onset of the deviation S' occurs at higher strength levels (and fracture probabilities) as the absolute cavity size (r/r_o) decreases. In the deviant regime, the fracture probabilities are lower and initially exhibit a stronger dependence on the fracture stress than anticipated by the shape parameter of the flaw size distribution, i.e., the effective m values are larger. Thereafter, below S", the fracture probabilities are identical to those obtained by considering the cavities as equivalent cracks.

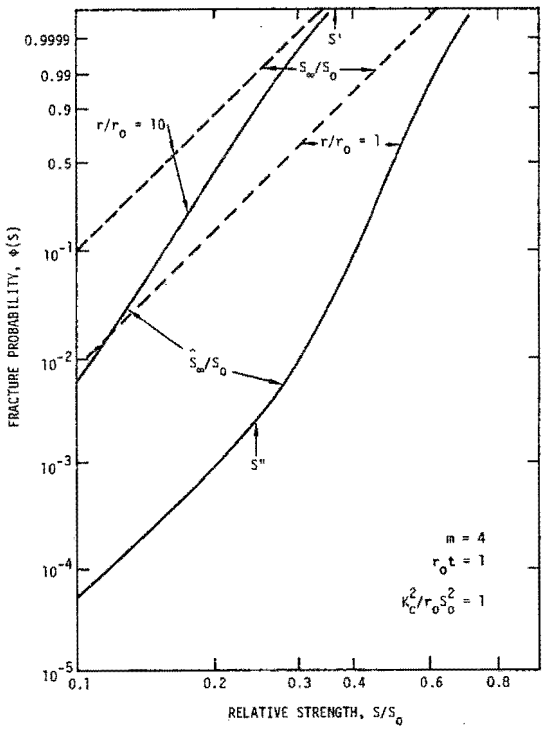

Fig. 7. The probability of fracture $\Phi(\hat{S}_\infty)$ from cylindrical cavities as a function of the relative strength ($\hat{S}_\infty/S_o$) plotted for three relative cavity radii, and for a shape parameter m of 4 ($r_o t_o$ and $K_c^2/r_o S_o^2$ are both unity); also plotted for comparison are the uniform stress results, $\Phi(S_\infty)$.

FRACTURE STUDIES

Concept

The applicability of the fracture relations derived in the preceding sections can only be adequately assessed if cavities with well-defined surface crack distributions are prepared and tested. Preliminary studies are reported for two types of cylindrical holes. The first set of samples contain holes prepared by drilling; these should contain surface cracks with a size distribution similar to that produced by surface grinding. The pertinent crack size distribution function for the hole might thus be estimated from separate strength tests on samples with ground surfaces. The second set of samples contain holes generated by incorporating W wires. The thermal expansion differential between W and Al_2O_3 should generate relatively well-defined radial cracks emanating from the W/Al_2O_3 interface. Further, since the W must be subsequently removed by oxidation, the expansion involved in the formation of the oxide causes additional crack extension, leaving a cylindrical cavity with relatively large radial cracks.

Experimental

The polycrystalline aluminum oxide material used for the fracture studies was prepared from Linde A aluminum oxide powder doped with 0.1 w/o magnesium oxide. The powders were milled in a

vibratory energy Sweco mill for 2 hr. using isopropyl and polyvinyl alcohols, and then dried for ~ 20 hrs. Consolidation was achieved by vacuum hot pressing at 1400°C for 1 hr. The resultant material was ~ 99% dense and had a grain size of ~ 2μm.

One set of samples was prepared by cutting rectangular (20 x 6.6 x 1.3 mm) beams from the hot-pressed disc, and rotary grinding the surfaces. Then, a through-thickness 0.7 mm radius hole was introduced into half of the samples (Fig. 8a) by diamond core drilling followed by reaming. The second set of samples was obtained by consolidating material containing a 127μm W wire. Rectangular beams were then cut such that the wire was in a through-width orientation (Fig. 8b). Finally, the W wire was removed by oxidizing in air for 2 hr. at 1150°C.

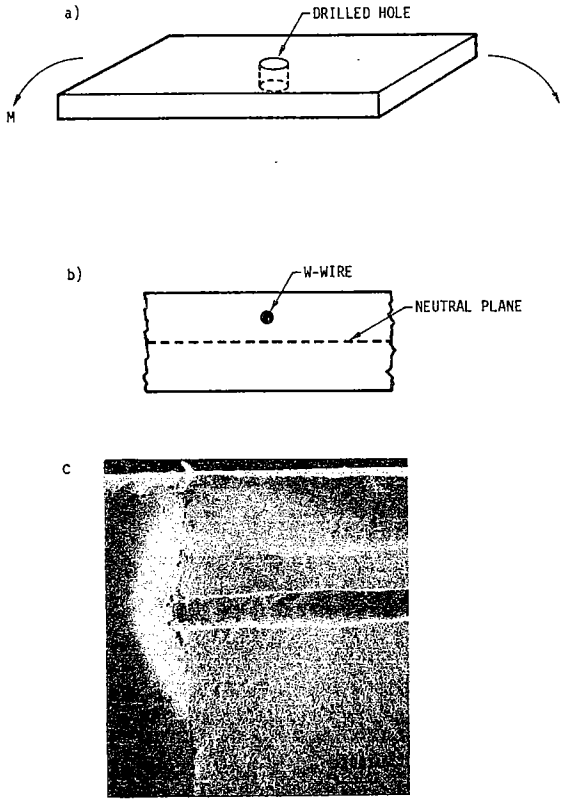

Fig. 8 (a) The drilled hole configuration.
(b) The hole configuration obtained using W wires.
(c) A fracture surface for a sample with a hole produced by a W wire; the initial length of the radial crack is indicated.

Strength tests were performed on each sample using a conventional four point flexure fixture with outer and inner spans of 19 and 6 mm, respectively. The tests were conducted in a dry nitrogen environment and at a rapid stress-rate (100 MPa s^{-1}), to minimize the influence of slow crack growth.[2] The fracture surface of each sample was examined in the optical or scanning electron microscope, in an attempt to identify the origin of fracture.

Results

The strength results obtained for the machined samples are plotted in Fig. 9. The results for the expansion induced cracks are summarized in Table I. As anticipated, the presence of the holes reduced the strength. Inspection of the samples containing the drilled holes indicated that the fracture always traversed the hole; but, fracture initiation could not always be unambiguously determined to occur from sites on the cavity surface. Examination of the fracture surfaces of the samples prepared with W wire indicated a clear demarkation of the profile of the radial crack that initiated failure (Fig. 8c).

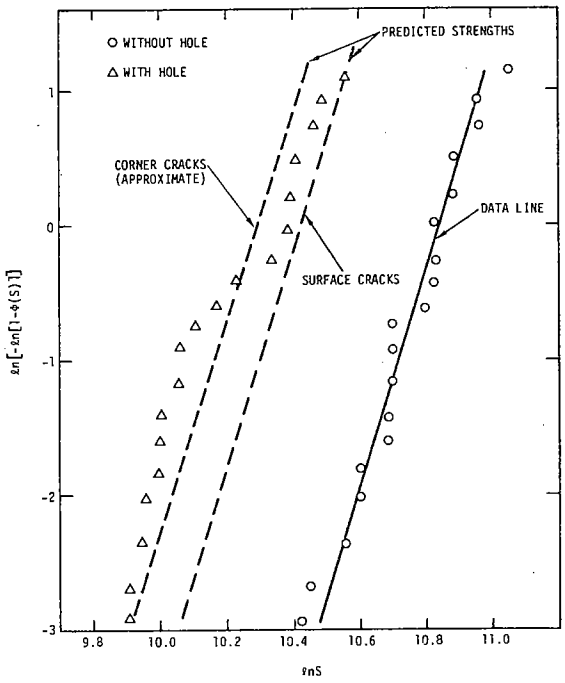

Fig. 9. A comparison of the fracture strengths of samples with and without drilled holes, showing the strengths of the latter predicted from the former.

TABLE I

STRENGTH RESULTS ON ALUMINA SAMPLES

WITH AS-FABRICATED HOLES

Fracture Probability (Φ=n/(N+1))	Fracture Strength (MPa)
0.14	183
0.29	190
0.43	204
0.57	230
0.71	251
0.86	254

The fracture toughness of the material was also determined, using the indentation technique.[8] For a load of 200N, the measured parameters were: indentation diameter, 100 μm; total crack length 250 μm. These values correspond to a toughness of 4.0 MPa $\sqrt{m}$.

Interpretation

(a) Drilled Cavities

For the samples without cavities, the fracture probability in four point flexure, for fracture occurring within the inner span, can be derived directly from Eqn. (6) as;

$$-\ell n\left[1-\Phi(\hat{S}_a)\right] = \left(\frac{\hat{S}_a}{S_o}\right)^m \left[\ell b + 2\ell \int_0^{d/2} \left(1 - \frac{2z}{d}\right)^m dz\right]$$

$$\equiv \left(\frac{\hat{S}_a}{S_o}\right)^m \ell \left[b + d/(m+1)\right] \qquad (13)$$

where ℓ is the inner span, b the sample width, d the sample depth, $\hat{S}_a$ the outer fiber stress at fracture and z the distance from the tensile surface (the first term in the parentheses relates to fracture from the tensile surface, and the second term allows for fracture from the side faces). For the samples containing the drilled cavities, the fracture probability (c.f. Eqn. (12)) is

$$-\ell n\left[1-\Phi(\hat{S}_H)\right] = \left(\frac{\hat{S}_H}{S_o}\right)^m$$

$$\left\{\left(\ell b - \pi r^2 + \frac{d\ell}{(m+1)}\right) + 4rA(m)Z^m(\alpha)\int_0^{d/2}\left(1 - \frac{2z}{d}\right)^m dz\right\}$$

$$\equiv \left(\frac{\hat{S}_H}{S_o}\right)^m \left\{\left(\ell b - \pi r^2 + \frac{d\ell}{(m+1)}\right) + \frac{2rdA(m)Z^m(\alpha)}{(m+1)}\right\} \qquad (14)$$

where $\hat{S}_H$ is the outer fiber stress at fracture, in the presence of the hole. The experimental results are interpreted in terms of Eqns. (13) and (14) by firstly obtaining the strength distribution parameters m and S_o, from a best fit of the data for the as-machined samples to Eqn. (13), as indicated by the data line on Fig. 9. Then, fracture probabilities in the presence of the hole can be derived for the same surface flaw population by inserting these distribution parameters and the pertinent A(m) and Z(α) values into Eqn. (14)(the α value pertinent to each strength level was evaluated by employing the measured polycrystalline K_c, of 4 MPa $\sqrt{m}$). The predicted strengths in the presence of the hole are plotted on Fig. 9. The predicted values conform relatively closely to the measured values at large probabilities ($\gtrsim$0.6), but afford a substantial underestimate at lower probabilities. To assess the possibility that fracture from corner sites (see Fig. 3) might be the origin of the discrepancy at low probabilities, the corner crack correction factor (Section 2) is applied to z, and the fracture probabilities re-evaluated. The results are plotted in Fig. 9. A much closer correspondence with the data at low fracture probabilities is apparent; suggesting that the fractures in the low probability regime occur primarily from corner sites. However, the fractographic evidence is not sufficiently definitive for this suggestion to be fully substantiated.

As an indication of the influence of the distribution parameter m on the strength reduction effected by a cylindrical hole, the strength ratio $\hat{S}_a/\hat{S}_H$ at constant probability is derived for the specific specimen geometry used in the present tests, and for a strength level of ~200 MPa (this ratio is independent of the scale parameter S_o). The results for a surface crack and a corner crack are plotted in Fig. 10. Note that the strength ratio always exceeds the value expected from the stress concentration factor (0.33).

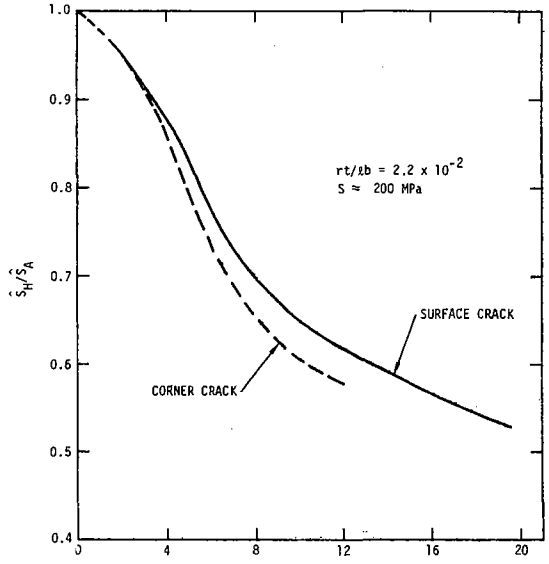

Fig. 10. The effect of the shape parameter, m, on the relative strengths of samples with and without drilled holes.

(b) Expansion Induced Cracks

The radial cracks generated by the fabrication of cavities from W wires appear to be ~2r in length (Fig. 8c). The stress intensity factor solutions (Fig. 1) would indicate that the cylindrical hole should exert a minor influence on the extension condition for radial cracks of this magnitude. However, several radial cracks of variable length emanate from each cavity (up to a maximum of 6). Also, the crack lengths are a significant fraction of the sample thickness. The quantitative interpretation of the measured fracture strength in the presence of these cracks is, therefore, a complex analytic problem. One sample, for which these complexities are minimized, has been chosen for analysis; this sample (strength 204 MPa) had five cracks, with the largest normal to the sample axis and the others at orientations $>\pi/4$. Fracture occurred from the crack normal to the sample axis (Fig. 8c). Initially, if the effects of the sample boundaries and the other radial cracks are neglected, the stress intensity factor at the crack front closest to the tensile surface is;

$$K_I = \sigma_o \left(\frac{2}{\pi a^*}\right)^{\frac{1}{2}} \int_0^{a^*} \frac{x^{\frac{1}{2}}}{(a^*-x)^{\frac{1}{2}}} \left[\frac{1-2(h+a^*-x)}{d}\right] dx$$

$$\equiv \sigma_o \left(\frac{\pi a^*}{2}\right)^{\frac{1}{2}} \left[\frac{1-(2h+a^*/2)}{d}\right] \qquad (15)$$

where $a^*=2(a+r)$, σ_o is the outer fiber stress and h is the distance between surface and the crack front. An approximate (upper bound) correction for the influence of the boundary can be deduced from Isida's results[19] for a strip containing an eccentric crack. For the present problem - a ligament width $h \sim 2a^*/3$ - the stress intensity factor at the upper crack front could be larger than that anticipated from Eqn. (15), by ~1.09. A maximum possible correction for the influence of the other radial cracks comes from Westman's solution[20] for the pressurized star crack; for 6 cracks, the correction is ~0.8.

Inserting the measured toughness (4 MPz μm), crack length (190 μm), hole radius (77 μm) and ligament depth (400 μm) into Eqn. (15), the fracture strength is predicted to be 207 MPa. The boundary correction decreases the predicted strength to a minimum of 190 MPa, while the crack interaction correction increases the strength to a maximum of 259 MPa. The latter cannot be reconciled with the measured strength (204 MPa), indicating that the crack interaction effect is of minor importance in this instance. Then, the relatively good correlation of the single crack solution with the measured strength tends to confirm that the pressure of the central hole had little influence on the crack extension condition.

IMPLICATIONS AND CONCLUSIONS

A method for predicting fracture probabilities, when fracture occurs from cavities, has been formulated by combining concepts from linear elastic fracture mechanics and from fracture statistics. The method has been applied to cylindrical cavities, using the best available fracture mechanics and statistics solutions. The same basic procedure can incorporate improved fracture mechanics solutions, as they emerge. The analysis demonstrates that fracture from cavities depends on the flaw population that exists at the cavity surface, the size of the flaws relative to the cavity radius and on the stress field around the cavity. The interpretation and prediction of fracture requires a detailed knowledge of each of these influences. Otherwise, the interpretation can only be subjective. This issue is addressed more extensively in the companion paper, in the context of fracture from spherical cavities.

Experimental results obtained on Al_2O_3 samples containing cylindrical cavities and relatively well-defined surface crack distributions indicated reasonable correspondence with the theory. The major uncertainties derive from inadequate stress intensity factor solutions for crack configurations of practical interest. This is an area for future study.

APPENDIX I

Defining S* as the flaw strength, or the applied stress needed to cause unstable crack extension, Eqn. (15) gives

$$\frac{K_c\sqrt{\pi}}{2S^*\sqrt{a}} = 1.07 + \frac{1.37}{0.52 + a/r} \qquad (A1)$$

Then, defining the apparent strength S as the strength of a flaw exposed to a uniform tension equal to that at the cavity surface;

$$S = \sqrt{\pi}\, K_c/7.38\sqrt{a} \qquad (A2)$$

Combining Eqns. (A1) and (A2) yields;

$$(S/S^*)^3 - (S/S^*)^2 + 0.12(S/S^*)\alpha - 0.032\alpha = 0 \qquad (A3)$$

where

$$\alpha = (1/r)(K_c/S^*)^2$$

Using the standard solution for a cubic equation then yields the relation for S/S* given by Eqn. (11).

ACKNOWLEDGEMENT

The authors are indebted to the Defense Advanced Research Project Agency for financial support, under Contract F33615-74-C-5180, and to Mr. J. Gysbers for his assistance in the numerical integration.

This research was sponsored by the Center for Advanced NDE, operated by the Science Center, Rockwell International, for the Defense Advanced Research Projects and the Air Force Materials Laboratory under Contract F33615-74-C-5180.

REFERENCES

1. See for example, R.W. Rice, Fracture Mechanics of Ceramics (Ed R.C. Bradt, D.P.H. Hasselman and F.F. Lange) Plenum, N.Y. 1974, p. 323.
2. A.G. Evans and T.G. Langdon, Prog. Mater. Sci. 21 (1976) p. 195.
3. O. Vardar, I. Finnie, D.R. Biswas and R.M. Fulrath, Int. J. Frac. 13 (1977) 215.
4. R.W. Davidge and G. Tappin, Proc. Brit. Ceram. Soc. 15 (1970) p. 47.
5. O.L. Bowie, Jnl. Maths and Physics 35,(1976) 60.
6. G.C. Sih, Handbook of Stress Intensity Factors (Lehigh Univ. Press) 1973.
7. R.C. Shah, "Mechanics of Crack Growth," ASTM STP 590 (1976) p. 429.
8. R.J. Hartranft and G.C. Sih, Mechanics of Fracture I (Ed. G.C. Sih) Noordhoff (1973) 179.
9. A.G. Evans and E.A. Charles, Acta Met 25 (1977) 919.
10. S. Timoshenko and J.N. Goodier, Theory of Elasticity (McGraw-Hill) 1951.
11. A.F. Grandt, Intl. Jnl. Frac. 11 (1975) 283.
12. A.S. Kobayashi and A.N. Enetanya, ASTM STP 590 (1976) 477.
13. J.R. Matthews, F.A. McClintock and W.A. Shack, Jnl. Amer. Ceram. Soc., 59 (1976) 304.
14. A.G. Evans and R.L. Jones, Jnl. Amer. Ceram. Soc., 61 (1978) 156.
15. W. Weibull, Jnl. Appl. Mech. 18 (1951) 193.
16. M. Adams and G. Sines, Jnl. Amer. Ceram. Soc. 59 (1976) 300.
17. A.G. Evans, Jnl. Amer. Ceram. Soc., May/June 1978, in press.
18. A.G. Evans and E.A. Charles, Jnl. Amer. Ceram. Soc. 59 (1976) 371.
19. M. Isida, "Methods of Analysis and Solutions of Crack Problems" (Ed. G.C. Sih) Noordhoff (1973) p. 56.
20. R.A. Westman, J. Maths. Phys. 43 (1964) 191.